Theory of plasmon-polaritons in binary metallic supercrystals

Arseniy Epishin,[1] Stephanie Reich,[1] and Eduardo B. Barros[2]
[1]*Department of Physics, Freie Universität Berlin, Arnimallee 14, 14195 Berlin, Germany*
[2]*Department of Physics, Federal University of Ceará, Fortaleza, Ceará 60455-760, Brazil*

(Received 2 February 2023; accepted 30 March 2023; published 12 June 2023)

We present a theory of optical excitations in binary plasmonic supercrystals that are made out of two types of metal nanoparticles. Compared to monodisperse supercrystals, binary crystals have a larger number of plasmonic bands. Their dispersion is governed by the lattice symmetry, unit cell parameters, and shape and material composition of the nanoparticle building blocks. We develop a quantum description of the plasmon polaritons in supercrystals that starts from the dipole and quadrupole excitations of the nanoparticles, their interaction, and their coupling to photons. We show how to use group theory to analyze the plasmon- and photon-induced supercrystal states and their interaction. Plasmon-polaritons of binary metallic supercrystals are in the regime of ultrastrong and deep strong light-matter interaction; i.e., the coupling strength is on the same order as the photon energy. One consequence of the strong interaction is that quadrupolar plasmon modes and photons with energies well above the plasmon energies have to be taken into account to calculate the polariton dispersion. A cesium chloride crystal of two nanoparticles with different dipole and quadrupole energies serves as the example structure to show how the plasmon-polariton dispersion depends on the properties of the nanoparticles and supercrystal structure. The tools presented here can be used to predict and analyze any type of optically active excitation in supercrystals. The results show how to differentiate the optical properties of binary nanoparticle supercrystals into properties that inflexibly depend on lattice symmetry and properties that can be finely tuned by choosing the nanoparticle composition and shape.

DOI: 10.1103/PhysRevB.107.235122

I. INTRODUCTION

Nanoparticle supercrystals are promising artificial materials for tailoring exquisite physical properties [1]. The properties of these three-dimensional arrangements of nanoparticles with long-range crystalline order [1–5] are determined by the interparticle interactions and can be controlled by the choice of the composing particles and their crystalline arrangement. Supercrystals composed of metallic nanoparticles have drawn considerable interest in the last few years [4–8] as they can be used to explore phenomena in the ultrastrong regime of light-matter coupling (USC) [4,6,9]. The optical or plasmonic excitations of the metallic nanoparticles give rise to plasmon-polaritons in the supercrystals that are propagating and collective excitations of the entire crystal lattice. Exciting the polaritons creates a dense pattern of electromagnetic hot spots of potential use in ultrasensitive analytic spectroscopy and photomediated catalysis [6,10]. We recently developed a quantum microscopic formalism appropriate to describe the plasmon-polaritons in metallic nanoparticle supercrystal and its dependence on key crystal parameters such as packing density and nanoparticle oscillator strength [11]. The model predicts the optical excitations of supercrystals, agreeing with experiments as well as numerical simulations based on finite difference methods.

So far the optical properties of plasmonic nanoparticle supercrystals have been studied for monodisperse nanoparticles and cubic structures [4,11,12]. We want to extend the description to binary supercrystals, in which there are two or more inequivalent sites in the crystal unit cell that naturally provide a much richer class of compositions and structures [13–17]. Just as atoms arranged in different crystalline lattices give rise to a wide range of properties, binary supercrystals offer more freedom in tailoring. Different from the case of the atomic crystals, the bonding between the nanoparticles in supercrystals is governed more by the surface-terminating ligands and less by the properties of the nanoparticles. This separates the choice of nanoparticle properties from their bonding in contrast to atoms as building blocks creating more freedom in manipulating the crystal properties. Previous theoretical work on binary supercrystals so far has focused on supercrystal self-assembly and structure [18–21]. When dealing with more complex crystal structures, the number of excitations increases leading to a large number of plasmon-polariton bands. The presence of so many different branches, each with their specific features, poses a major challenge for understanding the properties of this system and how it depends on the supercrystal parameters. For instance, one can use different materials and nanoparticle sizes for each site, tuning their resonance energies and coupling parameters in order to control the properties of the supercrystal. Furthermore, the fact that each particle can hold higher order multipole excitations, such as the quadrupole excitations discussed here, opens up a wider range of possibilities for matching the energies of the different excitations (dipole, quadrupole, and photon).

In this paper we show how to extend the microscopic description of plasmonic supercrystals to include structures with two or more atoms in the unit cell. We study the formation of plasmon-polaritons in nanoparticle supercrystals and its dependence on key parameters of the nanoparticles (dipole

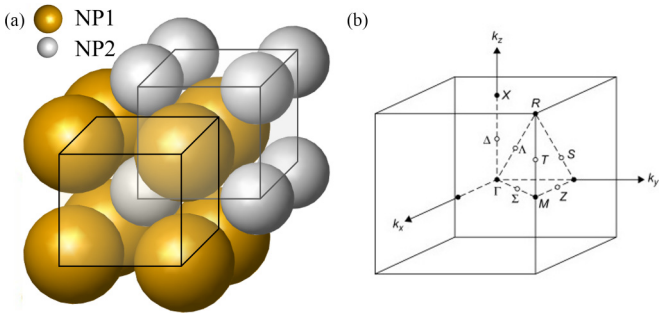

FIG. 1. (a) Nanoparticle supercrystal with caesium chloride structure in real space. NP1 is the particle with a large diameter and NP2 with a smaller diameter. (b) First Brillouin zone of the simple cubic lattice in reciprocal space. The high-symmetry points and lines are indicated with their usual labels.

and quadrupole energies, oscillator strength) and the crystal (packing density, lattice constants, crystal structure). We propose the use of the symmetry properties of the dipole and quadrupole plasmons in the supercrystals as a tool for tracking and understanding the physics of the plasmon-polariton excitations. Using the example of CsCl crystal structure, we show that introducing more than one particle into the unit cell can lead to interesting effects, such as lattice site localization of the modes. Furthermore, it provides several degrees of freedom for manipulating and tuning the physical properties of the supercrystal. This results in various plasmonic and polaritonic bands giving rise to a rich selection of combinations similar to the solid-state chemistry of the electrons in regular atomic crystals.

This paper is organized as follows. We first introduce in Sec. II the calculations in a chosen binary system and then present the group theory analysis for the symmetries of the photons and plasmon excitations in this particular crystal structure (Sec. III). With that in hand, we analyze the light-matter interaction on the dipole excitations (neglecting quadrupoles) and discuss how the interaction with the electromagnetic field affects the symmetry-related properties of these supercrystals. Finally, we include the quadrupole excitations and discuss how they interact with the dipoles and light, also from the perspective of their symmetry, and how these properties can be tailored by properly choosing the nanoparticle size and their composing materials.

II. PLASMON POLARITONS IN BINARY CRYSTALS

In most of this paper we will illustrate the plasmonic and polaritonic properties of nanoparticle supercrystals using the examples of the cesium chloride (CsCl) crystal structure. By this we mean an artificial lattice that is composed to two types of nanoparticles, NP1 and NP2, with different diameter, which are arranged like the cesium and chloride atoms in CsCl [Fig. 1(a)]. The CsCl structure consists of a simple cubic lattice with one atom or nanoparticle at the corner (NP1 in our case) and the other atom or nanoparticle in the center of the cubic unit cell (NP2). This structure is often mistaken as body-centered cubic, but the sites of its Bravais lattice are at the corner of the cube. The CsCl structure is similar to the more widely known NaCl structure, which has the same atomic basis but an FCC Bravais lattice. When the ions or nanoparticles are of similar size, the CsCl structure is adopted, but with increasing size difference ($r_2/r_1 < 0.5$) the NaCl structure becomes stable [22]. We selected the CsCl structure for our work because simple cubic is the most straightforward three-dimensional Bravais lattice and its first Brillouin zone is also simple cubic, allowing for a clear and straightforward analysis. The properties of other prototypical cubic structures will be discussed in a later study.

We are interested in the optical excitations of a lattice of two types of plasmonic nanoparticles that are arranged in the CsCl structure. The nanoparticles are characterized by their material and plasmon frequency as well as their radii r_1 (NP1) and r_2 (NP2). To calculate the plasmon-polariton band structure, we employ the formalism introduced in Ref. [11] where the total Hamiltonian is written as

$$\mathcal{H} = \mathcal{H}_M + \mathcal{H}_L + \mathcal{H}_{LM}. \tag{1}$$

$\mathcal{H}_M$ describes the matter Hamiltonian for the bare excitations of the nanoparticles, $\mathcal{H}_L$ gives the evolution of the free photons, and $\mathcal{H}_{LM}$ gives the light-matter interaction. The Hamiltonian for the matter part is

$$\mathcal{H}_M = \sum_{\sigma} \hbar\omega_\sigma b_{\mathbf{k},\sigma}, b^\dagger_{\mathbf{k},\sigma} + \sum_{\sigma,\sigma'} \hbar\sqrt{\Lambda_\sigma \Lambda_{\sigma'}} S^{\bar{\nu}\bar{\nu}'}_{\sigma\sigma'}(\mathbf{k}) \times (b_{\mathbf{k},\sigma} + b_{-\mathbf{k},\sigma})(b_{\mathbf{k},\sigma'} + b_{-\mathbf{k},\sigma'}), \tag{2}$$

where $\sigma = \{j, \nu\}$, with $j = 1, 2$ specifies the site in the unit cell and $\nu = x,\ y,\ z,\ x^2 - y^2,\ x^2 + y^2 - 2z^2,\ xy,\ yz,\ xz$ specify the dipole ($\bar{\nu} = D$) or quadrupole ($\bar{\nu} = Q$) bands. ω_σ is the bare energy for dipole and quadrupole excitations for each of the nanoparticles, and the factor $S^{\bar{\sigma}\bar{\sigma}'}_{\sigma\sigma'}(\mathbf{k})$ differs depending on whether $\bar{\sigma}$ is (j, D) for $\nu = x,\ y,\ z$ and (j, Q) for $\nu = x^2 + y^2 - 2z^2,\ xy,\ yz,\ xz$. Expressions for $S^{DD}_{\sigma\sigma'}$, $S^{DQ}_{\sigma\sigma'}$, and $S^{QQ}_{\sigma\sigma'}$ can be found in the Supplemental Material [23] and describe, in reciprocal space, the interaction between dipoles and quadrupoles in the crystal lattice. We also assume that the frequency of the plasmons in the metallic nanoparticles can described by the Drude model $\epsilon = \epsilon_\infty - \omega_p^2/\omega^2$. In the quasistatic approximation, these plasmon frequencies are

$$\omega_D = \frac{\omega_p}{\sqrt{\epsilon_\infty + 2\epsilon_m}} \tag{3}$$

and

$$\omega_Q = \frac{\omega_p}{\sqrt{\epsilon_\infty + (3/2)\epsilon_m}}, \tag{4}$$

where ϵ_m is the dielectric constant of the surrounding material. The coupling parameters Λ_σ are given by

$$\Lambda_{j,D} = \frac{9\epsilon_m \omega_{j,D}}{8\pi(\epsilon_\infty + 2\epsilon_m)} F_j \tag{5}$$

and

$$\Lambda_{j,Q} = \left(\frac{3}{4\pi}\right)^{5/3} \frac{5\epsilon_m \omega_{j,Q}}{12(\epsilon_\infty + (3/2)\epsilon_m)} F_j^{5/3}, \tag{6}$$

where $F_j = V_j/V_{uc}$ is the ratio between the particular nanoparticle volume (V_j) and the volume of the supercrystal unit cell (V_{uv}). The packing factor of the structure F can be obtained by the sum $F = \sum_j F_j$.

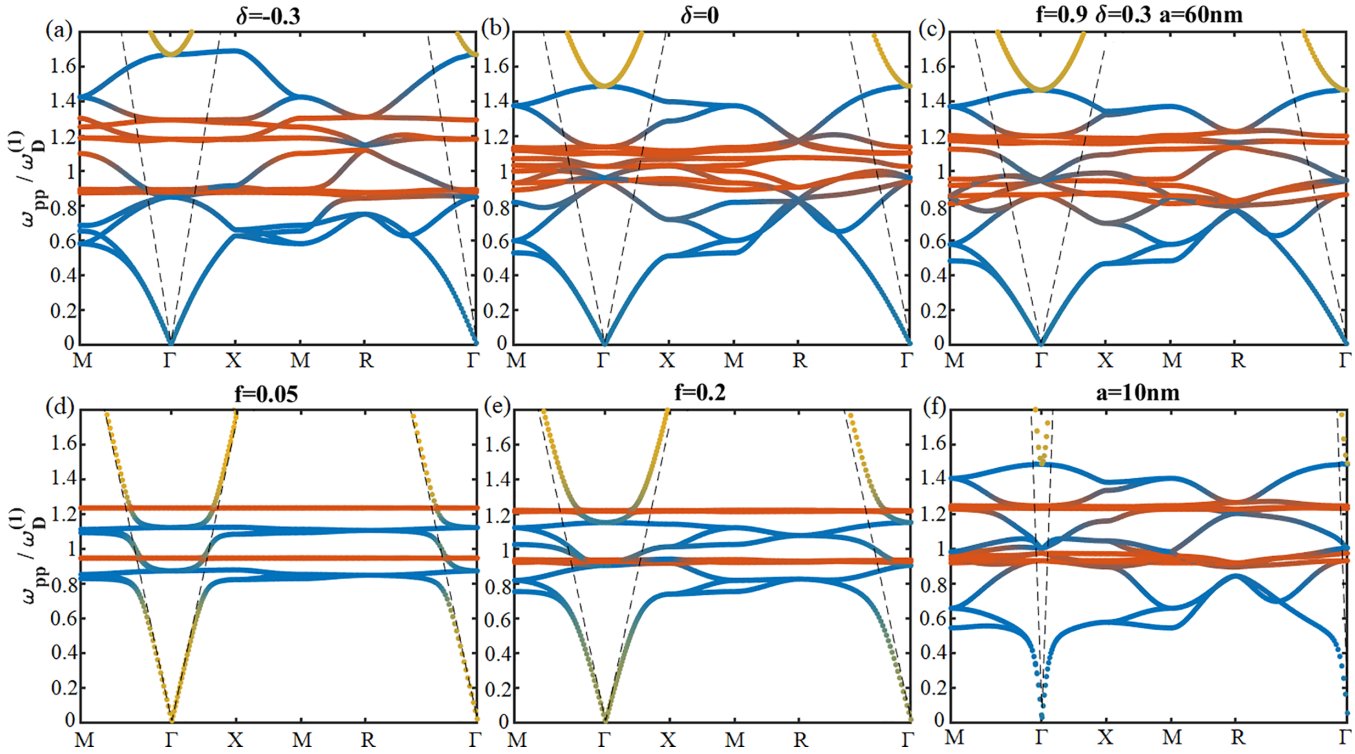

FIG. 2. Plasmon polariton dispersion of a CsCl supercrystal with different fill fraction f, nanoparticle plasmon frequency difference δ, and lattice parameter a. The bands are colored in accordance with the calculated contributions of dipole (blue), quadrupole (red), and photon (yellow) bare excitations to each of the states. Frequencies are plotted in units of the dipole frequency of NP1 that we set to $\omega_D^{(1)} = 2\pi c/a$. Dashed black lines show the uncoupled photon dispersion. (a) The larger nanoparticle has a higher dipole frequency ($\delta = -0.3$). (b) The nanoparticles have the same plasmon frequency ($\delta = 0$). (c) Parameters chosen for this work; see Fig. 3(a). The smaller particle has a higher plasmon frequency ($\delta = 0.3$), $f = 0.9$, and $a = 60$ nm in (a)–(c). (d) Very low fill fraction ($f = 0.05$); dipoles and quadrupoles are nondispersive. (e) Low fill fraction ($f = 0.2$); quadrupoles are nondispersive, but dipoles become dispersive and mix with photons. (f) Lattice parameter $a = 10$ nm, which leads to a photonic band with large dispersion.

The free photon Hamitonian is trivially described by $\mathcal{H}_L = \sum_{\mathbf{k},\lambda} \hbar\omega_{pt,\mathbf{k}} c_{\mathbf{k},\lambda} c^\dagger_{\mathbf{k},\lambda}$ while the light matter interaction is given by two parts $\mathcal{H}_{LM} = \mathcal{H}^{(1)}_{LM} + \mathcal{H}^{(2)}_{LM}$, with

$$\mathcal{H}^{(1)}_{LM} = i\hbar \sum_{\mathbf{k},\mathbf{G},\lambda,\sigma} \omega_{\bar{\nu}} \xi^{\sigma}_{\lambda,\mathbf{G}}(\mathbf{k})(b^\dagger_{-\mathbf{k},\sigma} - b_{\mathbf{k},\sigma}) \times (c_{-\mathbf{k}-\mathbf{G},\lambda} + c^\dagger_{\mathbf{k}+\mathbf{G},\lambda}) \tag{7}$$

and

$$\mathcal{H}^{(2)}_{LM} = \hbar \sum_{\mathbf{k},\lambda,\lambda',\mathbf{G},\mathbf{G}'} \Xi^{\lambda\lambda'}_{\mathbf{G},\mathbf{G}'}(\mathbf{k})(c^\dagger_{-\mathbf{k}-\mathbf{G}',\lambda'} + c_{\mathbf{k}+\mathbf{G}',\lambda'}) \times (c_{-\mathbf{k}-\mathbf{G},\lambda} + c^\dagger_{\mathbf{k}+\mathbf{G},\lambda}). \tag{8}$$

Here we defined

$$\xi^{\sigma}_{\lambda,\mathbf{G}}(\mathbf{k}) = \mathrm{f}_{\mathrm{D}}(|\mathbf{k}+\mathbf{G}|)\xi^{\mathrm{D}}_0(\mathbf{k})\mathrm{P}^{\mathrm{D}}_{\nu,\lambda}(\mathbf{k}+\mathbf{G}), \quad \text{for } \bar{\nu} = \mathrm{D}$$
$$\xi^{\nu}_{\lambda,\mathbf{G}}(\mathbf{k}) = i\mathrm{f}_Q(|\mathbf{k}+\mathbf{G}|)|\mathbf{k}+\mathbf{G}|\bar{R}\xi^{Q}_0(\mathbf{k})P^{Q}_{\nu,\lambda}(\mathbf{k}+\mathbf{G}) \text{ for } \bar{\nu} = \mathrm{Q} \tag{9}$$

and

$$\Xi^{\lambda\lambda'}_{\mathbf{G},\mathbf{G}'}(\mathbf{k}) = \sum_{\nu} \omega_{\bar{\nu}} \xi^{\nu*}_{\lambda'\mathbf{G}'}(\mathbf{k})\xi^{\nu}_{\lambda\mathbf{G}}(\mathbf{k}), \tag{10}$$

with the LM coupling parameter

$$\xi^{\bar{\nu}}_0(\mathbf{k}) = \sqrt{\frac{2\pi\,\Lambda_{\bar{\nu}}}{\omega_{pt}(\mathbf{k})}} \tag{11}$$

and polarization tensors

$$P^{D}_{\nu,\lambda}(\mathbf{k}) = \hat{e}_\nu \cdot \hat{e}_\lambda$$
$$P^{Q}_{\nu,\lambda}(\mathbf{k}) = \tfrac{1}{2}[\chi_\nu : \hat{e}_k\hat{e}_\lambda + \hat{e}_\lambda\hat{e}_k]. \tag{12}$$

Here χ_ν are the unit tensors for the quadrupoles [23]. The unit vector $\hat{e}_\lambda$ that specifies the photon polarization depends on $\mathbf{k}$. As in our previous work [11] we also introduce the form factors

$$\mathrm{f}_D = \frac{3}{(k\rho_j)^3}[\sin(k\rho_j) - k\rho_j\cos(k\rho_j)]$$
$$\mathrm{f}_Q = \frac{9}{(k\rho_j)^3}[\mathrm{Si}(k\rho_j) - \sin(k\rho_j)] \tag{13}$$

that take into account the finite size of the nanoparticles; $\mathrm{Si}(x)$ is the sine integral function.

Within the microscopic model, the plasmon-polaritons of the supercrystal are defined by three sets of parameters (see Fig. 2): the plasmonic modes of the nanoparticles, the fill fraction of the lattice, and the absolute value of the lattice constant. The first set of parameters is determined by the

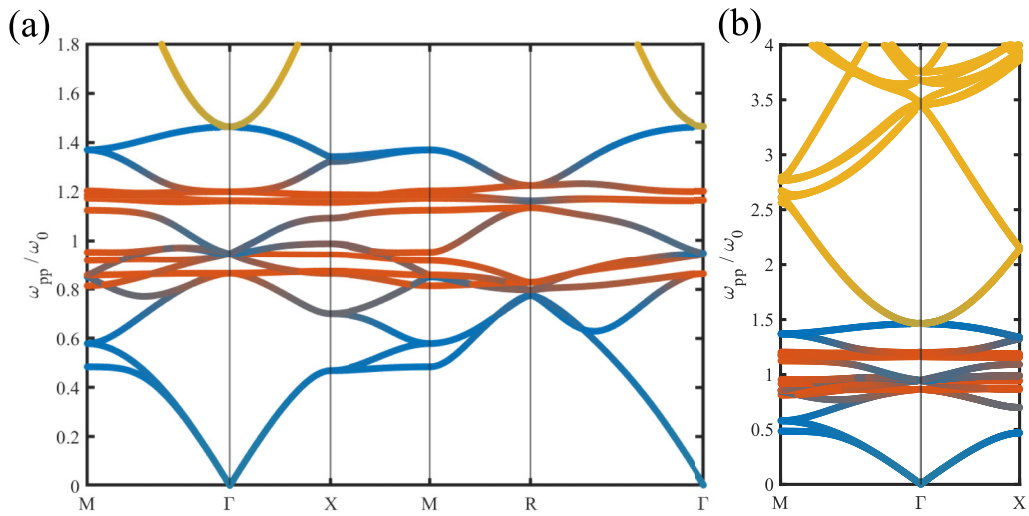

FIG. 3. (a) Plasmon polariton dispersion of a CsCl supercrystal. Fill factor $f = 0.9$; the frequencies of NP1 and NP2 differ by $\delta = 0.3$, lattice parameter $a = 60$ nm, $r_1 = fa/2$, $r_2/r_1 = 0.732$, $\epsilon_\infty = \epsilon_m = 1$. (b) Photons of higher wave vectors and energies are folded back into the first Brillouin zone and must be included in the calculation.

material composition of the nanoparticles (ω_p and ϵ_∞) and the surrounding medium (ϵ_m). This affects mainly the energy of the plasmon excitations (ω_D and ω_Q) and the maximum coupling (Λ) for each excitation in the nanoparticles. Moreover, since the two nanoparticles in the unit cell of a binary supercrystal are different, their plasmon frequencies may also differ [24,25], which strongly affects the dispersion relation; see Figs. 2(a)–2(c). To describe the different plasmon frequencies, we define δ such that $\omega_D^{(2)} = (1+\delta)\omega_D^{(1)}$. For negative values of δ [Fig. 2(a)], the dipole excitation energy for the larger particle $\omega_D^{(1)}$ is larger than for the smaller particle; for $\delta > 0$ the situation is reversed [Fig. 2(c)]. The second set of parameters is given by the size of the particles compared to the lattice parameter or, more precisely, by the relative fill factors F_j for each nanoparticle, which governs the coupling parameters between dipoles, quadrupoles, and photons. For simplicity, we work with a ratio between the particle radii $r_2/r_1 = 0.732$ throughout this paper, which yields the maximum packing factor for the CsCl structure $F_{\mathrm{CsCl}} = 0.729$. It is useful now to define the fill fraction $f = F/F_{\mathrm{CsCl}}$ as the ratio between the packing factor for a given choice of r_1 and r_2 and the maximum packing factor, because the CsCl structure is uniquely defined by f ($r_1 = fa/2$, $r_2 = 0.732fa/2$, and $F = 0.729f$). In Figs. 2(c)–2(e) we demonstrate how the dispersion relation changes based on the fill fraction f. If it is too small [Fig. 2(d)], dipole and quadrupole bands have no dispersion and little coupling to photons. In this work we use $f = 0.9$ in order to simulate crystals with deep strong light-matter coupling. The last parameter is the lattice constant a of the unit cell, which sets up the energy scale of the photons compared to the plasmon energies in the system; see Figs. 2(c) and 2(f).

For the simulations shown in this paper, we fixed the frequency of the dipole excitations of NP1 to $\omega_D^{(1)} = 2c\pi/a$. With this choice the wave vectors for photon energies $\hbar\omega_{pt,\mathbf{k}} = \hbar\omega_D$ lie in the middle of the first supercrystal Brillouin zone. We chose $\epsilon_\infty = \epsilon_m = 1$, so that $\omega_Q^{(1,2)} = 1.09\omega_D^{(1,2)}$ for both particles [Eqs. (3) and (4)]. With these choices, the supercrystals investigated here are fully determined by the parameters a, f, and δ.

The calculated plasmon-polariton dispersion relation for the CsCl lattice with $f = 0.9$ and $\delta = 0.3$ is shown in Fig. 3(a). The polariton states in Fig. 3 are superpositions of the photons and the excitations of the two different nanoparticles in the unit cell. For spherical nanoparticles, each particle contributes three degenerate dipole states and five degenerate quadrupole states, whereas the photon contributes two degenerate states within the first Brillouin zone. The Umklapp terms that represent photons of larger wave vector and energy are included in the calculation; see Sec. VI. They are folded into the first Brillouin zone within the reduced zone scheme, which leads to an even higher number of states [Fig. 3(b)].

The coupling between the nanoparticle excitation and light-matter interaction give rise to plasmon-polaritons with a large Rabi splitting between the mainly photonic (yellow) upper polariton branch at $1.46\omega/\omega_D^{(1)}$ at Γ and the dipole-like (blue) lower polariton branch. For this particular lattice, the Rabi splitting in the ΓR direction $\Omega_R(\Gamma R) = 0.68\omega_D^{(1)}$, leading to a reduced coupling $\eta = \Omega_R/\omega_D^{(1)} \sim 1.13$, well in the deep strong coupling regime [26]. Similar reduced coupling strengths are observed for the other high-symmetry directions. The dispersion relation contains many intermediate branches between 0.8 and 1.3 $\omega/\omega_D^{(1)}$ at Γ that are related to longitudinal dipole-like collective excitations (blue) and to quadrupole-derived (red) bands. The dispersion confirms that quadrupole excitations need to be included as they can strongly couple to the dipole excitations and to photons in the CsCl lattice and many other binary lattices. This is evidenced by the fact that the hue of the intermediate branches change from a deeper red, for the quadrupole-related collective modes that do not couple to the dipoles, to shades of purple, for the regions in which the dipole and quadrupole excitations mix.

TABLE I. Polariton symmetry in CsCl supercrystal. Listed are the symmetry of the photon and the dipole- and quadrupole-induced states in a CsCl binary supercrystal. The dipoles and quadrupoles were placed at the Wyckhoff positions of NP1 and NP2. The high-symmetry points and lines are indicated by their symbol and **k** vectors. The irreducible representations of the longitudinal direction for the photons are are given in parentheses for completeness.

Symmetry point			Dipole		Quadrupole	
Symbol	**k** vector	Photon	NP1 ($1a$)	NP2 ($1b$)	NP1 ($1a$)	NP2 ($1b$)
Γ	$(0,0,0)$	Γ_4^-	Γ_4^-	Γ_4^-	$\Gamma_3^+ \oplus \Gamma_5^+$	$\Gamma_3^+ \oplus \Gamma_5^+$
X	$(0,0,1/2)$	$X_5^- (\oplus X_2^-)$	$X_3^- \oplus X_5^-$	$X_1^+ \oplus X_5^+$	$X_1^+ \oplus X_2^+ \oplus X_4^+ \oplus X_5^+$	$X_2^- \oplus X_3^- \oplus X_4^- \oplus X_5^-$
R	$(1/2,1/2,1/2)$	R_4^-	R_4^-	R_5^+	$R_3^+ \oplus R_5^+$	$R_3^- \oplus R_4^-$
M	$(1/2,1/2,0)$	$M_5^- (\oplus M_2^-)$	$M_3^- \oplus M_5^-$	$M_2^- \oplus M_5^-$	$M_1^+ \oplus M_2^+ \oplus M_4^+ \oplus M_5^+$	$M_1^+ \oplus M_3^+ \oplus M_4^+ \oplus M_5^+$
$\Delta = \overline{\Gamma X}$	$(0,0,u)$	$\Delta_5 (\oplus \Delta_1)$	$\Delta_1 \oplus \Delta_5$	$\Delta_1 \oplus \Delta_5$	$\Delta_1 \oplus \Delta_2 \oplus \Delta_3 \oplus \Delta_5$	$\Delta_1 \oplus \Delta_2 \oplus \Delta_3 \oplus \Delta_5$
$\Sigma = \overline{\Gamma M}$	$(u,u,0)$	$\Sigma_3 \oplus \Sigma_4 (\oplus \Sigma_1)$	$\Sigma_1 \oplus \Sigma_2 \oplus \Sigma_3$	$\Sigma_1 \oplus \Sigma_2 \oplus \Sigma_3$	$2\Sigma_1 \oplus \Sigma_2 \oplus \Sigma_3 \oplus \Sigma_4$	$2\Sigma_1 \oplus \Sigma_2 \oplus \Sigma_3 \oplus \Sigma_4$
$\Lambda = \overline{\Gamma R}$	(u,u,u)	$\Lambda_3 (\oplus \Lambda_1)$	$\Lambda_1 \oplus \Lambda_3$	$\Lambda_1 \oplus \Lambda_3$	$\Lambda_1 \oplus 2\Lambda_3$	$\Lambda_1 \oplus 2\Lambda_3$
$T = \overline{MR}$	$(1/2,1/2,u)$	$T_5 (\oplus T_1)$	$T_1 \oplus T_5$	$T_3 \oplus T_5$	$T_1 \oplus T_2 \oplus T_3 \oplus T_5$	$T_1 \oplus T_3 \oplus T_4 \oplus T_5$
$Z = \overline{MX}$	$(u,1/2.0)$	$Z_3 \oplus Z_4 (\oplus Z_1)$	$Z_1 \oplus Z_3 \oplus Z_4$	$Z_1 \oplus Z_2 \oplus Z_4$	$2Z_1 \oplus Z_2 \oplus Z_3 \oplus Z_4$	$Z_1 \oplus Z_2 \oplus Z_3 \oplus 2Z_4$
$S = \overline{RX}$	$(u,1/2,u)$	$S_3 \oplus S_4 (\oplus S_1)$	$S_1 \oplus S_2 \oplus S_3$	$S_1 \oplus S_3 \oplus S_4$	$2S_1 \oplus S_2 \oplus S_3 \oplus S_4$	$S_1 \oplus S_2 \oplus 2S_3 \oplus S_4$

III. GROUP THEORY ANALYSIS

We analyze the symmetry properties of plasmon-polaritons in the exemplary binary lattice that has a CsCl structure to show how the interaction and hybridization of the dipole, quadrupole, and photonic states is controlled by the lattice structure. The basic idea we follow in this section is to first establish the symmetry of the matter excitations induced by the localized plasmon modes and the photons at the various points of the Brillouin zone. We examine the mutual interaction of the dipole and quadrupole-derived collective states. For the photons, we will discuss how to describe the high-energy Umklapp states within the framework of group theory.

The group $\mathcal{G}_S$ of the CsCl structure is the symmorphic space group Pm-3m (221) or O_h^1 [27,28]. Each nanoparticle occupies one of two inequivalent Wyckoff positions $1a$ (NP1) and $1b$ (NP2) [29]. The Brillouin zone is also cubic and has four inequivalent high-symmetry points Γ, X, R, and M; see Fig. 1(b). For the plasmons, the multipole excitations of isolated spherically symmetric nanoparticles can be described in terms of the spherical harmonics and their symmetries. For the dipole excitations, the irreducible representations (irreps) should transform as that of the linear displacement (x, y, z), while the quadrupole excitations behave as the irreps of the traceless quadratic displacements $(x^2 - y^2,\ x^2 + y^2 - 2z^2,\ xy, xz, yz)$.

In a supercrystal of a given crystal structure the nanoparticles (NPs) occupy specific positions (Wyckoff positions) that are of the same or lower symmetry than the crystal itself; this reduces the full rotational symmetry of the individual NP to the symmetry of the Wyckoff position. At the highest symmetry Γ point, dipole excitations transform according to Γ_4^- (E_u) and quadrupole excitations as Γ_3^+ and Γ_5^+ (E_g and T_{2g}) [30]. For a given wave vector **k** in the first Brilloin zone, the spatial modulation of the wave function may further lower the symmetry associated with the Wyckoff position. In this case the relevant group is also the group of the wave vector **k**, defined within the first Brillouin zone ($\mathcal{G}_\mathbf{k}$). This is a subgroup of the space group of the crystal ($\mathcal{G}_S$), which can be obtained by selecting all operations in $\mathcal{G}_S$ that leave **k** invariant by a translation of a reciprocal lattice, i.e., which takes $\mathbf{k} \to \mathbf{k} + \mathbf{G}$. We should point out that the group of $\mathbf{k} + \mathbf{G}$ is isomorphic to that of **k**, a fact that will be important when dealing with the Umklapp photons. In Table I we show the irreps of the dipole and quadrupole excitations for the particles in the Wyckoff positions of NP1 and NP2 in the CsCl structure for selected (high-symmetry) points and lines of the first Brillouin zone.

For the photon part, the symmetry of the electromagnetic field is described in terms of the Poincaré group, which includes translations, rotations, and relativistic boosts [31]. Therefore, the light Hamiltonian is also invariant upon any spatial translations or rotations (within the rest frame of the crystal structure), including all of those in $\mathcal{G}_S$. The electromagnetic field can be thought to transform as a vector within a quasistatic approximation, and thus also behave as the Γ_4^- (E_u) irrep at the Γ point. However, the electromagnetic field in the Coulomb gauge has only two components (both perpendicular to **k**). It cannot be described by a threefold degenerate state. Furthermore, photons are not well defined at $\mathbf{k} = 0$. This problem is solved by moving away slightly from the Γ point and lowering the symmetry, leading to irreducible representations of lower dimensions. One of the representations will be one-dimensional and associated with the longitudinal direction. We list them in Table I in parentheses for completeness. The other two polarization directions are transverse in character. Depending on the high-symmetry points and lines they may be twofold degenerate or belong to nondegenerate representations; see Table I. The R point of the reciprocal lattice of CsCl structure is characterized by a group of the wave vector which is isomorphic to that of the Γ point (O_h point group), where a vector transforms as the three-dimensional R_4^- irrep. This irreducible representation is such that the longitudinal and transverse directions are, in principle, interchangeable. In spite of that, the selection rules for the photon-plasmon interaction can still be obtained by assuming that the photon transforms as a vector.

The first-order light-matter interaction term depends linearly on the vector potential $\mathbf{A}$ and is given by Eq. (7). The coupling of the dipole- and quadrupole-induced plasmonic states to photons can be obtained directly from Table I by identifying the dipole and quadrupole modes that transform as the same irrep as the photon for each high-symmetry position. We will discuss the results in Secs. IV and V. For the interaction between the electromagnetic field and matter excitations that are characterized by the wave vector $\mathbf{k}$, the relevant group is also the group of the wave vector $\mathbf{k}$, defined within the first Brillouin zone ($\mathcal{G}_\mathbf{k}$). Plasmon-polaritons with wave vector $\mathbf{k}$ should also transform according to the little group $\mathcal{G}_\mathbf{k}$. When considering the contribution of photons with $\mathbf{k}_{pt} = \mathbf{k} + \mathbf{G}$, however, the symmetry of the crystal is preserved only if all photon wave vectors in the star of $\mathbf{k} + \mathbf{G}$ are also taken into consideration. Failure to comply with this condition unphysically breaks the symmetry of the crystal. For weakly coupled systems the photons in the star of $\mathbf{k}_{pt}$ which are outside of the first Brillouin zone of the crystal have a much larger energy compared to the photons inside of the Brillouin zone, and their interaction can be disregarded. This is not the case for strongly coupled systems, and one must make sure to include photons with $\mathbf{G} \neq 0$ in order to avoid unphysical results.

The effect of the Umklapp terms becomes especially important when considering the polarization of photons with wave vectors $\mathbf{k}_{pt}$ outsize of the first Brillouin zone (1BZ). These photons get folded into the 1BZ by the translational symmetry, which affects the orientation of their wave vector and polarization. To illustrate this we take an alternative perspective and repeat the 1BZ throughout the crystal, fixing the direction of polarization of the plasmons, instead of folding the photons into the 1BZ. Since the irreps of the matter states at $\mathbf{k}$ and $\mathbf{k} + \mathbf{G}$ are the same, the analysis becomes much simpler. The direction of the wave vector $\mathbf{k} + \mathbf{G}$ (and of the photon polarization) is different from that of $\mathbf{k}$. This affects symmetry-imposed coupling of plasmons and photons and between photons. For instance, a photon with wave vector $\mathbf{k}_x\hat{\mathbf{x}}$ is polarized along the y or z direction. It should not couple to dipole plasmons polarized along x. However, a photon with wave vector $k_x\hat{\mathbf{x}} + 2\pi/a\hat{\mathbf{y}}$ has a polarization component along the x direction and may couple to x polarized plasmons. This leads to a weak but nonzero coupling between longitudinal plasmons and photons through the first-order light-matter interaction term when Umklapp processes are considered.

Finally, we discuss coupling by the second-order term in the light-matter interaction Hamiltonian. It is proportional to $|\mathbf{A}|^2$ and couples different photon states; see Eq. (8). This coupling originates from a summation of the products of photons with wave vectors $\mathbf{k} + \mathbf{G}$ and $\mathbf{k} + \mathbf{G}'$ and polarizations λ and λ' to the matter excitations ν. In a sense, this term is a measure of the correlation between photons due to the interaction with the plasmonic states or matter-induced photon-photon interaction. The $|\mathbf{A}|^2$ term is invariant under any symmetry operation of the crystal, thus transforming as the totally symmetric representation Γ_1 (A_{1g}). The term vanishes if λ is perpendicular to λ'. This condition is trivially obeyed for $\mathbf{G} = \mathbf{G}'$; however, for $\mathbf{G} \neq \mathbf{G}'$ this may not be true as $\hat{e}_\lambda$ and $\hat{e}'_\lambda$ depend on the relative orientation of the wave vectors of $\mathbf{k} + \mathbf{G}$ and $\mathbf{k} + \mathbf{G}'$, so that coupling between different polarizations becomes possible.

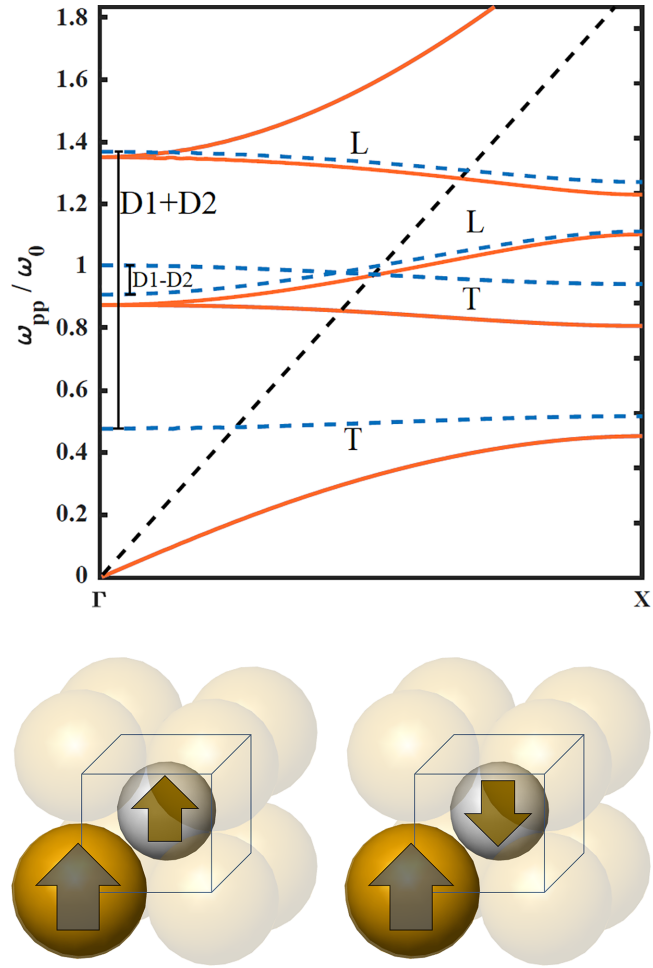

FIG. 4. Top: Dispersion along the plasmon-polariton $\Delta(\Gamma X)$ direction in a CsCl nanoparticle supercrystal (solid orange) and uncoupled plasmonic (dashed blue) and photonic (dashed black) states. Bottom: Symmetric (D1+D2) and antisymmetric (D1-D2) combinations of the dipoles in the CsCl lattice unit cell.

The most important result of our group theory analysis is the set of selection rules based on the irreducible representations of the multipole excitations, collected in Table I. These rules guide which bands will exist, mix, and become degenerate independently of the nanoparticle material properties. Throughout this work we will use these selection rules to confirm and interpret the results of our quantum microscopic model. Another important conclusion is that in order to preserve the crystal symmetry, we must consider Umklapp processes and include photons with large wave vectors in our calculation.

IV. DIPOLE BANDS

In the preceding sections we developed the numerical and group-theory tools to study the formation of plasmon-polaritons in nanoparticle supercrystals. In this section we focus on the dipole excitations of the nanoparticles and how they lead to collective states and couple to the electromagnetic field. Figure 4 shows the dispersion relation for the dipole-derived plasmon bands (blue dashed lines) and the photons

(black dashed) in the $\Delta = \overline{\Gamma X}$ direction without considering light-matter interaction. The solid (orange) lines represent the plasmon-polariton bands, i.e., including light-matter coupling. Along the $\Delta = \overline{\Gamma X}$ high-symmetry line, the uncoupled photon dispersion is composed of one twofold degenerate band transforming as the Δ_5 irrep. The dipole states are composed of four bands (Table I): two twofold degenerate states for the transverse dipole modes Δ_5 and two Δ_1 bands for the longitudinal modes. As the bands approach $k = 0$, the symmetry of the CsCl lattice dictates that they merge into two threefold degenerate states transforming as the Γ_4^- irrep (Table I). However, this does not happen when neglecting light-matter coupling. Instead, we find a splitting of the longitudinal and transverse states (LT splitting) of $\sim\omega_D^{(1)}$ for the symmetric and $\sim 0.1\omega_D^{(1)}$ for the antisymmetric combinations of the dipoles in the CsCl lattice unit cell (Fig. 4). Longitudinal-transverse splitting is a well-known phenomenon that is observed in all systems with dipole-like excitations from optical phonons to excitons [32–34]. The deviation from the predicted threefold degenerate states at the Γ point was explained by the formation of an anisotropic macroscopic field, splitting the longitudinal and transverse bands [35]. As we show now, this explanation is not necessary because the inclusion of light-matter interaction leads to the predicted degeneracy (Fig. 4) and fully restores the integrity of the symmetry analysis.

Including light-matter interaction leads to the formation of five plasmon-polariton bands (Fig. 4 solid lines). Along the Δ direction the lower (LPP) and upper (UPP) plasmon polariton bands are doubly degenerate and belong to the Δ_5 irrep. In the intermediate region, there are a twofold degenerate band (the second lowest band) and two longitudinal nondegenerate bands that interact very weakly with light. The number and the type of irreducible representations remain unchanged by light-matter interaction. For both the coupled and and the uncoupled case the symmetry analysis predicts five bands belonging to the Δ_1 and Δ_5 irreps; see Table I. As these bands approach the Γ point they merge into the predicted threefold degenerate Γ_4^- state. After including light-matter interaction, the supercrystal excitations comply to the conditions imposed by the symmetry of the supercrystal. There is no need to introduce *a posteriori* a macroscopic electric field. This fact has been pointed out before for the LO-TO splitting of phonon-polaritons [36], but it is interesting to see that it appears to be a more general concept for polariton bands.

Another prediction of the group theory analysis in Table I is that in some high-symmetry directions the dipole bands induced by each of the particles have different symmetries and are forbidden to mix. For example, in the $T = \overline{MR}$ direction, the dipole centered on NP1 transforms like $T_1 \oplus T_5$, while the dipole on NP2 belongs to $T_3 \oplus T_5$. We thus expect one plasmonic band along T that has only contributions from the first nanoparticle and one band with contributions only from the second nanoparticle. Figures 5(b) and 5(c) show the contribution of the dipoles on NP1 (D1) and NP2 (D2) to the plasmon polaritons along the Z-T or $\overline{XML}$ high-symmetry path; see Fig. 1(b). The thickness of the line indicates the contribution of the nanoparticle plasmons to each of the bands. The lowest energy band in Fig. 5(b) transforms as the Z_3 and T_1 irreducible representations and has contributions only from

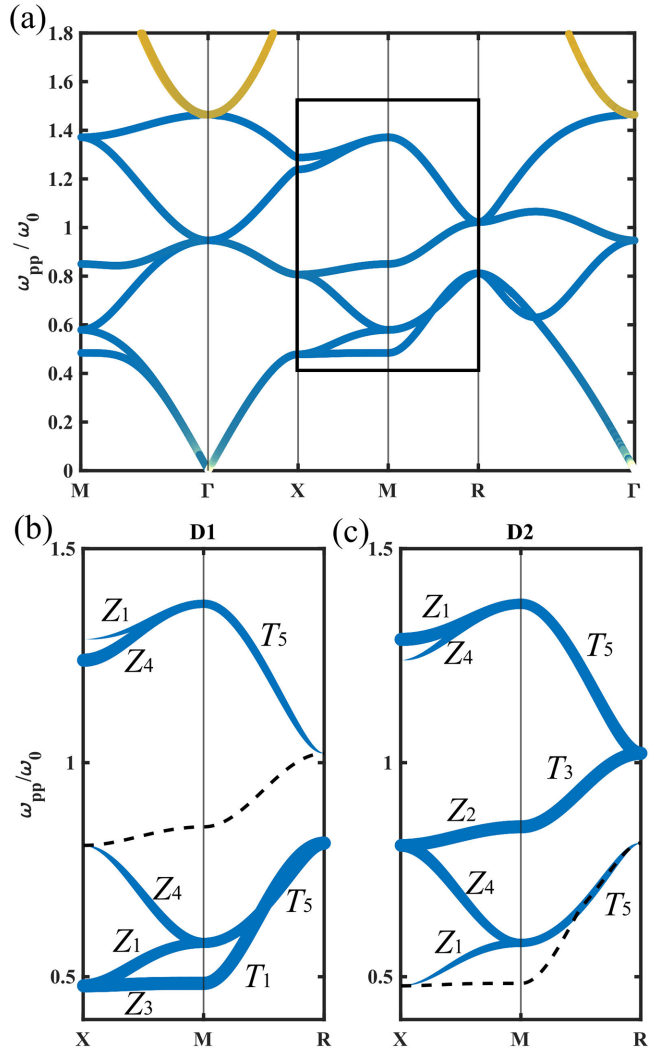

FIG. 5. (a) Plasmon polariton dispersion relation without including quadrupoles. The highlighted part is decomposed into dipole excitations of the larger (b) and the smaller (c) nanoparticle. Dashed lines show bands that have no contribution from the respective nanoparticle.

the plasmons of NP1. On the other hand, the third band from the bottom in Fig. 5(c) (crossing the M point at $\sim 0.8\omega_D^{(1)}$) has Z_2 and T_3 symmetry and is localized on the NP2 sites. This is in contrast to a double set of bands that have Z_1 and Z_4 irreps and merge into twoold degenerate T_5 bands, since they have contributions from both particles as expected from the analysis in Table I.

V. QUADRUPOLE BANDS

The higher-order modes of plasmonic nanoparticles do not interact with electromagnetic fields within the quasistatic approximation and are considered dipole forbidden excitations. Collective modes of nanoparticle agglomerates that are induced by the higher-order modes of the individual nanoparticles, however, are often dipole active and may mix with the dipole-derived collective states [37]. A mixing of the dipole and quadrupole-derived plasmonic band and their coupling to photons was already observed in fcc crystals [11]. In the CsCl

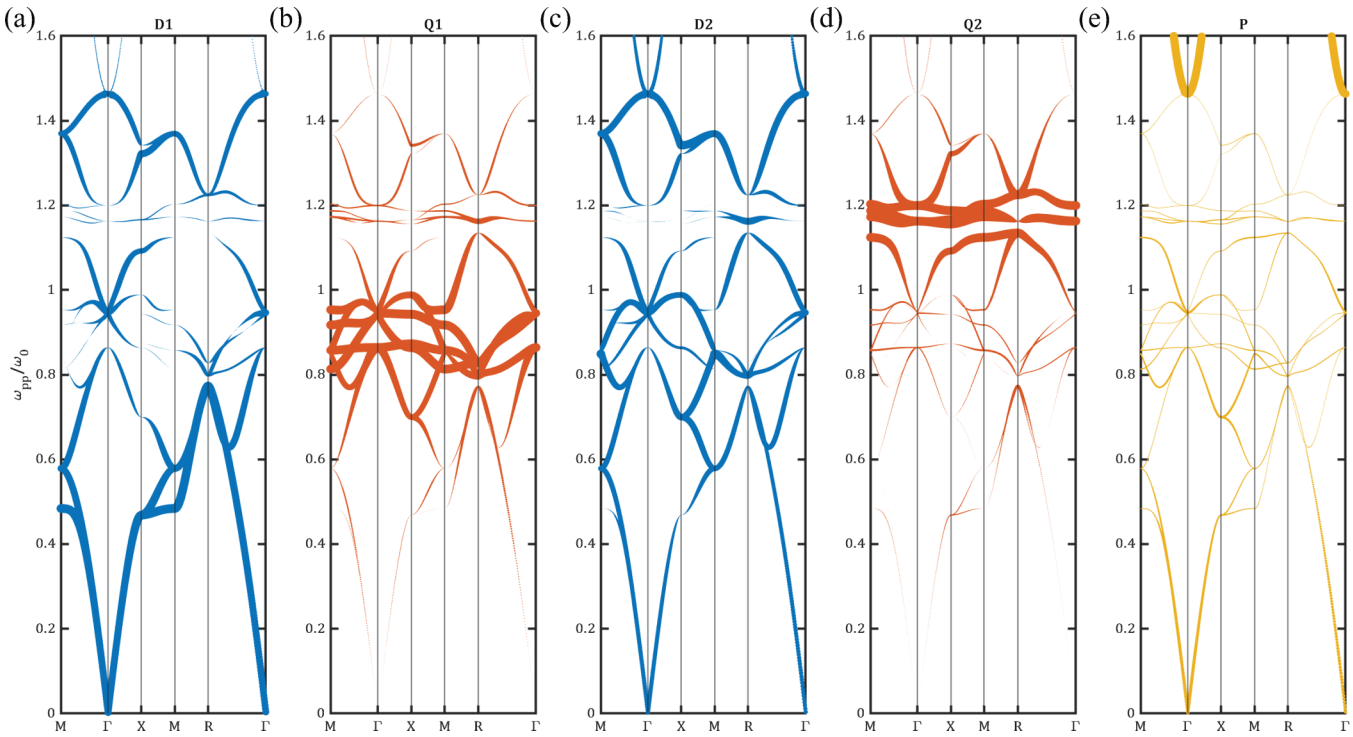

FIG. 6. CsCl supercrystal dispersion, decomposed into contributions. (a) Dipole contribution from the larger particle. (b) Quadrupole contribution from the larger particle. (c) Dipole contribution from the smaller particle. (d) Quadrupole contribution from the smaller particle. (e) Photon contribution. $f = 0.9$, $\delta = 0.3$, $a = 60$ nm.

structure dipole-quadrupole mixing is forbidden at the Γ and *R* point, but allowed at least for some of the states throughout the rest of the Brillouin zone (Table I).

As the dipole-quadrupole and quadrupole-quadrupole interactions are much weaker than dipole-dipole coupling, the quadrupole-derived bands appear nearly flat in Fig. 3(a) with little dispersion. If the quadrupole excitations of the two particles differ in energy, the two sets of quadrupole-derived bands appear almost independent. This is evident in Fig. 6, where despite the dense packing ($f = 0.9$) there is little overlap between the quadrupole contributions of the the lattice sites ($Q1$ and $Q2$), because of their energy difference ($\delta = 0.3$). This is in contrast to the strongly dispersive dipole-derived bands, except if mixing is prohibited by symmetry (as discussed in the previous section). The weak interaction between the hybrid dipole-quadrupole states and the photons [Fig. 6(e)] indicates that the dispersion of these intermediate bands is mainly governed by matter-matter coupling. The interaction between dipole and quadrupole bands is allowed only for states which transform according the the same irreducible representation of the group of the wave vector for that particular point in the Brillouin zone. For instance, at the Γ and *M* point dipoles and quadrupoles transform as different irreps and thus cannot mix. In the other high-symmetry directions, dipoles and quadrupoles induced from either site share the same irreps and mix to form hybrid states. The detailed analysis of this mixing for specific directions is left for a future publication, but it can be straightforwardly deduced by matching irreps for dipoles and quadrupoles in Table I.

When the quadrupole and dipole bands have comparable energy *D*-*Q* hybrid states may change from predominantly dipole-like to quadrupole-like as one moves through the Brillouin zone. The dipole-quadrupole and quadrupole-quadrupole interactions are tunable by materials composition of the nanoparticles. In our simulation the quadrupole excitation energy of the larger particle ($Q1$) nearly matches the energy of the dipole excitations of the smaller particle ($D2$), which promotes *D*-*Q* mixing between $Q1$ and $D2$ in the bands with $\omega_{pp} = 0.8\text{-}1\omega_D^{(1)}$ in Fig. 6. The quadrupole of the smaller particle ($Q2$) interacts more weakly with the dipoles becoming less dispersive and more confined to the energy region near $\omega_{pp} = 1.2\omega_D^{(1)}$ [Fig. 6(d)].

We now study how the polaritons depend on the frequency mismatch between NP1 and NP2. In Fig. 7 we show the plasmon polariton energies for a fixed k along Δ as a function of δ. The color of the bands indicates their dipole, quadrupole, or photon nature. For the full dispersion relation at $\delta = -0.3$, 0 and 0.3, see Figs. 2(a)–2(c). The dipole bands are strongly mixed into bonding and antibonding combinations; they also couple strongly to the photons even for large values of $|\delta|$. For this reason, the dipole- and photon-related bands show a nearly parabolic dispersion with δ. For instance, the top two bands in Fig. 7(a) correspond to the bonding longitudinal dipole (blue) and the upper polariton (yellow) state that are degenerate at Γ but split away from zero (Fig. 4). The energies of these states follow a parabolic behavior with a minimum for $\delta_{\text{min}} < 0$. This behavior is understood from the perspective of the longitudinal plasmon, which mainly involves dipole-dipole interactions. The particles contribute proportional to δ. The interaction between the two particles adds a contribution to the Hamiltonian that scales as $\pm\delta^2$, where $\pm$ is for the bonding-and antibonding configurations. At the minimum

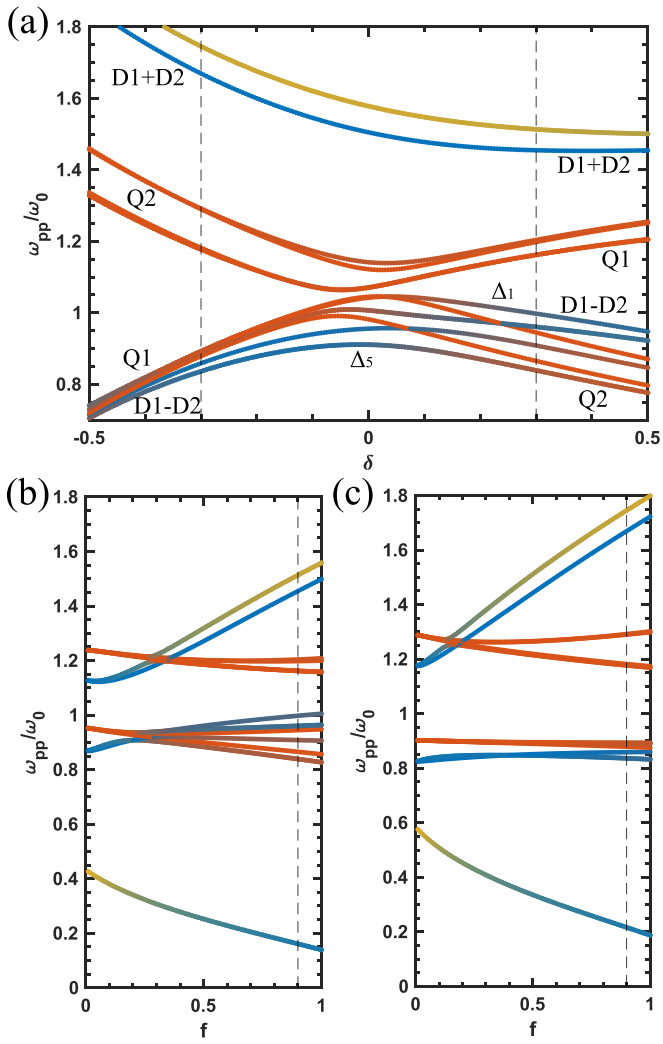

FIG. 7. (a) Dependence of the plasmon-polariton energies on δ for $\mathbf{k} = 0.25\Gamma X$ and $f = 0.9$. The colors indicate the dipole, quadrupole, and photon contributions to each of the states. (b) Dependence of the plasmon-polariton energies on f for $\mathbf{k} = 0.25\Gamma X$ and $\delta = -0.3$. (c) Dependence of the plasmon-polariton energies on f for $\mathbf{k} = 0.25\Gamma X$ and $\delta = 0.3$.

energy these two effects cancel; the minimum depends on the relative packing factors F_j of the particles. A similar dependence is expected for the other dipole-related plasmon-polariton bands; however, their exact behavior is changed by the dipole-photon and dipole-quadrupole interaction. The lower dipole-related bands (with energy $\sim 0.92\omega_D^{(1)}$ for $\delta = 0.5$) correspond to the antibonding longitudinal and transverse bands, which are also degenerate at Γ (Γ_4^-) and transform as the Δ_1 and Δ_5 irreducible representations for k in the Δ direction; see Fig. 4.

In contrast to the dipole bands, the quadrupole bands are not strongly mixed for large $|\delta|$. For instance, for $\delta = 0.5$ the top quadrupole bands mainly originate from the larger particles $Q1$, whereas the bottom quadrupole bands originate from the smaller particles $Q2$. As δ decreases, the $Q2$ states move up in energy and mix with the antibonding dipoles if they belong to the same representation (Δ_1, Δ_5). These are the bands that change from red to blue for $\delta < 0.4$ in Fig. 7(a). As δ gets closer to zero, the $Q1$ and $Q2$ form bonding and antibonding quadrupole states. As δ increases further into positive values, the quadrupoles start to separate again into mainly $Q1$ (lower energies) and $Q2$ (higher energies). Also, the energy of the antibonding dipoles start to move away from that of the quadrupoles leading to a much weaker dipole-quadrupole coupling for this particular $\mathbf{k}$.

We can also tune the dipole-quadrupole interaction by changing the fill fraction f. In Fig. 7(b) we fix $\delta = 0.3$ and vary $f = 0$–1, finding that the DQ interaction increases with f. Full dispersion relation at different fill fractions is shown in Figs. 2(c)–2(e). The lower quadrupole band, composed mainly of states that originate from NP2, is strongly affected by the interaction with the dipoles, leading to mixed dipole-quadrupole bands that spread over a wide energy region. On the other hand, the top quadrupole bands are weakly affected by dipole-quadrupole and quadrupole interactions. This is expected since the main contribution to DQ mixing comes from the interaction between an excitation in one nanoparticle with the other nanoparticle, so that the excitations of the smaller particle NP2 are more sensitive to the larger dipole moments of NP1. The situation is reversed for $\delta = -0.3$; see Fig. 7(c) and Fig. 2(a). In this case the top quadrupole band originates from NP2; it is strongly affected by DQ and QQ interactions, whereas the bottom quadrupole state remains almost independent of f. Similar effects are observed for other values of $\mathbf{k}$ throughout the Brillouin zone, suggesting the possibility of finely tuning the supercrystal properties and promoting dipole-quadrupole coupling for specific wave vectors.

VI. PHOTONS

Finally, we turn our attention to the photons. Essentially, all polariton states contain contributions by photons [Fig. 6(e)] with the highest contribution in the transverse upper polariton close to $\omega_{pp} = 1.2\omega_D^{(1)}$ in Fig. 6(e). The latter is the consequence of the deep strong light-matter coupling in the supercrystal simulated in Fig. 6 and will be discussed later. The finite contribution of the photons to the longitudinal plasmon-polaritons may be surprising at first. After all, photons are transverse in polarization. This contribution originates from the coupling with high-energy photons in Umklapp processes, which also explains the photon coupling to nondipolar plasmon states. Briefly, in addition to $\mathbf{G} = 0$ states, the light-matter interaction Hamiltonian $\mathcal{H}_{LM}$ takes into account photons with $\mathbf{G} \neq 0$. They represent photons with $\mathbf{k}_{pt}$ outside of the first Brillouin zone that are folded into this zone by the crystal translational symmetry; see Fig. 3(b). The contribution of these states to the polariton band structure is usually disregarded due to their much higher energy. For supercrystals in the ultrastrong and deep strong coupling regimes, however, light-matter interaction is on the same order as the photon energy, and photon wave vectors (and energies) outside the first Brillouin zone must be taken into account. This is especially true for the symmetry-related properties of these systems and the polarization of the plasmons and photons as discussed in Secs. III and IV. We found that we need to include at least eight Brillouin zones in the calculation in order to reach convergence and properly describe the plasmon-polariton states.

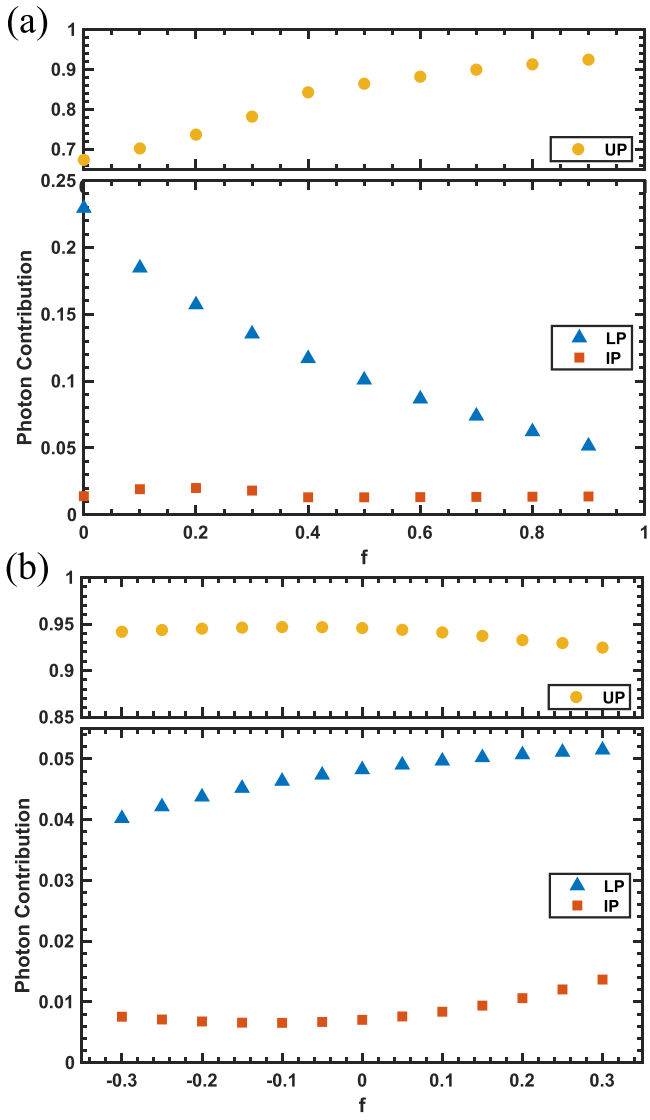

FIG. 8. Relative contribution of photons to the plasmon-polaritons as a function of f (for $\delta = 0.3$) and as a function of δ (for $f = 0.9$). The relative contribution is calculated considering the high-symmetry path around the Brillouin zone. LP refers to the bottom two bands which form the lower polariton, UP refers to the top two bands in Fig. 3, and IP refers to all the intermediate modes between the two.

In Fig. 8 we show the mean contributions of photons to the lower, intermediate, and upper polaritons as a function of f and δ. The photon contribution to the lower polariton decreases with increasing f [see Fig. 8(a)] as was previously observed for the fcc lattice [11]. This is a manifestation of the decoupling of light and matter due to the A^2 term in the interaction Hamiltonian [26,38]. The upper polariton is mainly composed of photons with increasing f. Finally, the photon contribution to the intermediate bands is much smaller and almost independent of the fill fraction, indicating that light-matter interaction has only a weak effect on these modes. The intermediate bands are mainly composed of longitudinal modes or are antibonding combinations of transverse modes. Both types of modes will not couple strongly to light, the first due to the fact that light is transverse and the second due to the reduced effective dipole of the antibonding combinations. To verify this, we plot in Fig. 8(b) the average contribution of photons to the bands as a function of δ for $f = 0.9$. The photonic character of the intermediate polaritons is largest for large $|\delta|$ because of the different plasmon frequencies of the dipoles and quadrupoles. The minimum contribution occurs for $\delta < 0$ due to the fact that the particles in the two sites have different size and thus different dipole moments.

VII. CONCLUSIONS

In conclusion, we studied the plasmon-polariton dispersion for a binary nanoparticle supercrystal. We further developed a microscopic model that contains the dipole and quadrupole modes of the nanoparticle building blocks and their coupling to photons to simulate structures with more than one particle per unit cell, significantly increasing the amount of bands. We used group theory to obtain selection rules for the photon-plasmon interaction and predict such behaviors as degeneracy and mixing of the dipole and quadrupole-derived states, demonstrating the dependence of the plasmon-polariton dispersion on symmetry-related properties of the crystal structure. We verified the necessity of including quadrupoles into plasmon-polariton calculation, as they can strongly couple to dipole excitations and photons even when the individual particles are well described by the quasistatic approximation. Photons with wave vectors outside the first Brillouin zone must be taken into account when simulating plasmonic supercrystals. Our methods can be applied to different lattice configurations with multiple particles in the basis, permitting a broad investigation into the symmetry properties and excitations of binary nanoparticle supercrystals. Furthermore, with this model we were also able to change the material attributes of the structure, such as nanoparticle plasmon frequency and fill fraction, which strongly affect light-matter interaction and the mixing of bands of different origin, suggesting that such structures may be finely tuned to achieve a desired optical response.

ACKNOWLEDGMENTS

We acknowledge funding and support from the European Commission through the Consolidator Grant DarkSERS (772108) and the Deutsche Forschungsgemeinschaft (DFG, 504656879). E.B.B. acknowledges financial support from CNPq, CAPES (finance code 001), and FUNCAP (PRONEX PR2-0101-00006.01.00/15). This work was supported by and partly carried out in the Research Building SupraFAB at Freie Universität Berlin (funded by BMBF, State of Berlin and Freie Universität Berlin).

[1] M. A. Boles, M. Engel, and D. V. Talapin, Self-assembly of colloidal nanocrystals: From intricate structures to functional materials, Chem. Rev. **116**, 11220 (2016).

[2] M. J. Murray and J. V. Sanders, Close-packed structures of spheres of two different sizes II. The packing densities of likely arrangements, Philos. Mag. A **42**, 721 (1980).

[3] C. B. Murray, C. R. Kagan, and M. G. Bawendi, Synthesis and characterization of monodisperse nanocrystals and close-packed nanocrystal assemblies, Annu. Rev. Mater. Sci. **30**, 545 (2000).

[4] N. S. Mueller, Y. Okamura, B. G. M. Vieira, S. Juergensen, H. Lange, E. B. Barros, F. Schulz, and S. Reich, Deep strong light-matter coupling in plasmonic nanoparticle crystals, Nature (London) **583**, 780 (2020).

[5] F. Schulz, O. Pavelka, F. Lehmkühler, F. Westermeier, Y. Okamura, N. S. Mueller, S. Reich, and H. Lange, Structural order in plasmonic superlattices, Nat. Commun. **11**, 3821 (2020).

[6] N. S. Mueller, E. Pfitzner, Y. Okamura, G. Gordeev, P. Kusch, H. Lange, J. Heberle, F. Schulz, and S. Reich, Surface-enhanced Raman scattering and surface-enhanced infrared absorption by plasmon polaritons in three-dimensional nanoparticle supercrystals, ACS Nano **15**, 5523 (2021).

[7] D. García-Lojo, S. Núñez-Sánchez, S. Gómez-Graña, M. Grzelczak, I. Pastoriza-Santos, J. Pérez-Juste, and L. M. Liz-Marzán, Plasmonic supercrystals, Acc. Chem. Res. **52**, 1855 (2019).

[8] M. Blanco-Formoso, N. Pazos-Perez, and R. A. Alvarez-Puebla, Fabrication of plasmonic supercrystals and their SERS enhancing properties, ACS Omega **5**, 25485 (2020).

[9] D. Baranov, B. Munkhbat, E. Zhukova, A. Bisht, A. Canales, B. Rousseaux, G. Johansson, T. J. Antosiewicz, and T. Shegai, Ultrastrong coupling between nanoparticle plasmons and cavity photons at ambient conditions, Nat. Commun. **11**, 2715 (2020).

[10] M. Herran, S. Juergensen, M. Kessens, D. Hoeing, A. Köppen, A. Sousa-Castillo, W. J. Paraand, H. Lange, S. Reich, F. Schulz, and E. Cortés, Plasmonic bimetallic two-dimensional supercrystals for H_2 generation, Nat. Catal. (to be published).

[11] E. B. Barros, B. G. Vieira, N. S. Mueller, and S. Reich, Plasmon polaritons in nanoparticle supercrystals: Microscopic quantum theory beyond the dipole approximation, Phys. Rev. B **104**, 035403 (2021).

[12] S. Lamowski, C.-R. Mann, F. Hellbach, E. Mariani, G. Weick, and F. Pauly, Plasmon polaritons in cubic lattices of spherical metallic nanoparticles, Phys. Rev. B **97**, 125409 (2018).

[13] P. Pusey and W. van Megen, Phase behaviour of concentrated suspensions of nearly hard colloidal spheres, Nature (London) **320**, 340 (1986).

[14] P. Bartlett, R. H. Ottewill, and P. N. Pusey, Superlattice Formation in Binary Mixtures of Hard-Sphere Colloids, Phys. Rev. Lett. **68**, 3801 (1992).

[15] E. V. Shevchenko, D. V. Talapin, C. B. Murray, and S. O'Brien, Structural characterization of self-assembled multifunctional binary nanoparticle superlattices, J. Am. Chem. Soc. **128**, 3620 (2006).

[16] E. V. Shevchenko, D. V. Talapin, N. A. Kotov, S. O'Brien, and C. B. Murray, Structural diversity in binary nanoparticle superlattices, Nature (London) **439**, 55 (2006).

[17] D. V. Talapin, E. V. Shevchenko, M. I. Bodnarchuk, X. Ye, J. Chen, and C. B. Murray, Quasicrystalline order in self-assembled binary nanoparticle superlattices, Nature (London) **461**, 964 (2009).

[18] A. Travesset, Binary nanoparticle superlattices of softparticle systems, Proc. Natl. Acad. Sci. USA **112**, 9563 (2015).

[19] A. Travesset, Topological structure prediction in binary nanoparticle superlattices, Soft Matter **13**, 147 (2017).

[20] A. Travesset, Soft skyrmions, spontaneous valence and selection rules in nanoparticle superlattices, ACS Nano **11**, 5375 (2017).

[21] I. Coropceanu, M. A. Boles, and D. V. Talapin, Systematic mapping of binary nanocrystal superlattices: The role of topology in phase selection, J. Am. Chem. Soc. **141**, 5728 (2019).

[22] M. Watanabe, M. Tokonami, and N. Morimoto, The transition mechanism between the CsCl-type and NaCl-type structures in CsCl, Acta Cryst. A **33**, 294 (1977).

[23] See Supplemental Material at http://link.aps.org/supplemental/10.1103/PhysRevB.107.235122 for dipole structure function.

[24] N. G. Bastús, J. Comenge, and V. Puntes, Kinetically controlled seeded growth synthesis of citrate-stabilized gold nanoparticles of up to 200 nm: Size focusing versus Ostwald ripening, Langmuir **27**, 11098 (2011).

[25] J. Piella, N. G. Bastús, and V. Puntes, Size-controlled synthesis of sub-10-nanometer citrate-stabilized gold nanoparticles and related optical properties, Chem. Mater. **28**, 1066 (2016).

[26] A. Frisk Kockum, A. Miranowicz, S. De Liberato, S. Savasta, and F. Nori, Ultrastrong coupling between light and matter, Nat. Rev. Phys. **1**, 19 (2019).

[27] T. Inui, Y. Tanabe, and Y. Onodera, *Group Theory and Its Application in Physics* (Springer, Berlin, Heidelberg, 1990).

[28] M. S. Dresselhaus, G. Dresselhaus, and A. Jorio, *Group Theory Application to the Physics of Condensed Matter* (Springer, Berlin, Heidelberg, 2008).

[29] M. I. Aroyo, A. Kirov, C. Capillas, J. M. Perez-Mato, and H. Wondratschek, Bilbao crystallographic server. II. Representations of crystallographic point groups and space groups, Acta Cryst. A **62**, 115 (2006).

[30] L. Elcoro, B. Bradlyn, Z. Wang, M. G. Vergniory, J. Cano, C. Felser, B. A. Bernevig, D. Orobengoa, G. de la Flor, and M. I. Aroyo, Double crystallographic groups and their representations on the Bilbao crystallographic server, J. Appl. Cryst. **50**, 1457 (2017).

[31] S. Weinberg, *The Quantum Theory of Fields: Volume 3, Supersymmetry* (Cambridge University Press, Cambridge, 1995).

[32] K. Huang, Lattice vibrations and optical waves in ionic crystals, Nature (London) **167**, 779 (1951).

[33] M. H. Cohen and F. Keffer, Dipolar sums in the primitive cubic lattices, Phys. Rev. **99**, 1128 (1955).

[34] M. M. Denisov and V. P. Makarov, Longitudinal and transverse excitons in semiconductors, Phys. Stat. Sol. (b) **56**, 9 (1973).

[35] P. Y. Yu and M. Cardona, *Fundamentals of Semiconductors Physics and Materials Properties* (Springer-Verlag, Berlin, Heidelberg, 1996).

[36] A. Quattropani, L. C. Andreani, and F. Bassani, Quantum theory of polaritons with spatial dispersion: Exact solutions, Nuovo Cimento D **7**, 55 (1986).

[37] N. S. Mueller, B. G. M. Vieira, F. Schulz, P. Kusch, V. Oddone, E. B. Barros, H. Lange, and S. Reich, Dark interlayer plasmons in colloidal gold nanoparticle bi- and few-layers, ACS Photon. **5**, 3962 (2018).

[38] S. De Liberato, Light-Matter Decoupling in the Deep Strong Coupling Regime: The Breakdown of the Purcell Effect, Phys. Rev. Lett. **112**, 016401 (2014).